ELSEVIER

Nuclear Instruments and Methods in Physics Research A 482 (2002) 693–706

NUCLEAR INSTRUMENTS & METHODS IN PHYSICS RESEARCH Section A

www.elsevier.com/locate/nima

Response of CsI(Tl) scintillators over a large range in energy and atomic number of ions. Part II: calibration and identification in the INDRA array

M. Pârlog[a,b], B. Borderie[b,*], M.F. Rivet[b], G. Tăbăcaru[a,b], A. Chbihi[c], M. Elouardi[d], N. Le Neindre[e], O. Lopez[e], E. Plagnol[b], L. Tassan-Got[b], G. Auger[c], Ch.O. Bacri[b], N. Bellaize[e], F. Bocage[e], R. Bougault[e], B. Bouriquet[c], R. Brou[e], P. Buchet[f], J.L. Charvet[f], J. Colin[e], D. Cussol[e], R. Dayras[f], A. Demeyer[g], D. Doré[f], D. Durand[e], J.D. Frankland[c], E. Galichet[b,h], E. Genouin-Duhamel[e], E. Gerlic[g], S. Hudan[c], D. Guinet[g], P. Lautesse[g], F. Lavaud[b], J.L. Laville[c], J.F. Lecolley[e], C. Leduc[g], R. Legrain[f], M. Louvel[e], A.M. Maskay[g], L. Nalpas[f], J. Normand[e], J. Péter[e], E. Rosato[i], F. Saint-Laurent[c,1], J.C. Steckmeyer[e], B. Tamain[e], O. Tirel[c], E. Vient[e], C. Volant[f], J.P. Wieleczko[c]

[a] *National Institute for Physics and Nuclear Engineering, RO-76900 Bucharest-Măgurele, Romania*
[b] *Institut de Physique Nucléaire, IN2P3-CNRS, F-91406 Orsay, Cedex, France*
[c] *GANIL, CEA et IN2P3-CNRS, B.P. 5027, F-14076 Caen, Cedex, France*
[d] *Laboratoire de Physique Nucléaire Appliquée, Kenitra, Maroc*
[e] *LPC, IN2P3-CNRS, ISMRA et Université, F-14050 Caen, Cedex, France*
[f] *DAPNIA/SPhN, CEA/Saclay, F-91191 Gif sur Yvette, Cedex, France*
[g] *Institut de Physique Nucléaire, IN2P3-CNRS et Université, F-69622 Villeurbanne, Cedex, France*
[h] *Conservatoire National des Arts et Métiers, F-75141 Paris, Cedex 03, France*
[i] *Dipartimento di Scienze Fisiche e Sezione INFN, Università di Napoli "Federico II", I80126 Napoli, Italy*

INDRA collaboration

Received 15 May 2001; received in revised form 24 July 2001; accepted 24 July 2001

Abstract

The light output of the 324 CsI(Tl) scintillators of INDRA has been measured over large ranges in energy: 1–80 AMeV and in atomic number of incident ions: $Z = 1$–60. An analytical expression for the non-linear total light response as a function of the energy and the identity of the ion is developed. It depends on four parameters. For three of them, connected to CsI(Tl) intrinsic characteristics, fixed values are proposed. Two applications are presented: energy

*Corresponding author. Tel.: +33-1-69157148; fax: +33-1-69154507.
E-mail address: borderie@ipno.in2p3.fr (B. Borderie).
[1] Present address. DRFC/STEP, CEA/Cadarache, F-13018 Saint-Paul-lez-Durance Cedex, France.

PII: S0168-9002(01)01712-0

calibration and fragment identification in telescopes using a CsI(Tl) crystal as residual energy detector.

PACS: 29.40.Mc; 32.50.+d

Keywords: Light response of CsI(Tl) to heavy ions; Quenching; δ-rays

1. Introduction

INDRA is a 4π axially symmetrical array for the detection of light and heavy charged nuclear reaction products [1,2] covering huge dynamic ranges, both in energy (from ≈ 1 MeV to ≈ 6 GeV) and in atomic number (from proton to uranium). It has a high granularity and a shell structure, consisting of several detection layers. For the last layer, which should stop all particles and fragments produced, thallium-activated caesium iodide scintillators (CsI(Tl)) coupled to photomultiplier tubes were chosen.

The calibration procedure for CsI(Tl) consists in finding a function L depending not only on the energy, but also on the identity of the particle, which describes the induced scintillation Q_0. The parameters of this function are determined by a global fit procedure which simultaneously compares the calculated scintillator response to the experimental one for all particles and fragments of well-known energies. The total scintillation is reconstructed by software, starting from two measured signal fractions, as shown in Sections 2 and 3. Afterwards, one may get a reference map for the identification of the reaction products in a two-dimensional plot showing ΔE—the energy deposited in the preceding detection layer—versus the total light from the CsI(Tl) crystal.

For the forward angles of INDRA ($3^\circ < \theta < 45^\circ$, rings 2–9), the detection layers which precede the scintillators consist of gas ionization chambers (ICs) and 300 μm silicon detectors. The Si detectors allowed an accurate determination of the residual energy—as presented in Section 2.2—for all fragments passing through and stopped in the scintillators. Thus, there is a tremendous set of data which facilitated a detailed study of the CsI(Tl) crystal light response. The exact expression of the total light output of a CsI(Tl) crystal, as predicted by the recombination and nuclear quenching model (RNQM) [3], implies a numerical integration over the energy and this fact is prohibitive for application purposes. Under suitable approximations, the integration may be analytically performed and a very easy to handle expression is deduced. The 3 or 4 involved parameters are determined. Except for the gain parameter, proper to each scintillator crystal and its electronic chain, the values of the other fit parameters, connected to intrinsic CsI(Tl) crystal properties, are fixed. Procedures for fragment identification in a $\Delta E - Q_0$ telescope-type map and for the energy calibration of the scintillator are developed and critically analyzed in Section 4, containing the RNQM applications.

For the backward angles of INDRA ($45^\circ < \theta < 176^\circ$, rings 10–17), the scintillators are preceded only by ionization chambers. The calibration of the scintillators leans on the above-mentioned light response expression and the CsI(Tl) characteristic parameter values, found at forward angles; the individual gain parameter is determined by means of light charged particle and eventually light fragment data. The calibration so found allows to safely extrapolate the charge identification in a $\Delta E - Q_0$ map to regions where no ridge lines are visible because of very low statistics, improving then both charge and energy determination for heavy fragments ($Z \geqslant 15$) detected beyond 45° with INDRA. Details are given in Section 4.

Our findings are summarized in Section 5.

Notation and values of physical constants and variables used in this paper. See also those in the preceding paper [3]. (Most of the notations of the original references have been kept.)

Notation

Experimental light output and related variables

t	time	s
$i(t)$	signal at the last dynode of the CsI(Tl) photomultiplier (PMT)	a.u. s^{-1}
Q_f	integral charge of the fast component of the signal	a.u.
τ_f	decay time constant of the fast component	s
Q_s	integral charge of the slow component of the signal	a.u.
τ_s	decay time constant of the slow component	s
Q_{fs}	integral charge corresponding to the whole signal	a.u.
$i_{mes}(t)$	measured signal at the output of the PMT anodic circuit	a.u. s^{-1}
Q_0	approximate total integrated charge $\propto$ experimental light output	a.u.
τ_0	decay time constant	s
τ_{0min}	lower value of the decay time constant	s
τ	rise-time constant at output of the PMT	s
F	experimental charge integrated in the "fast" gate	a.u.
S	experimental charge integrated in the "slow" gate	a.u.

Calculated light output and related variables

$C_{e,n}$	constants in the approximative expressions of $S_{e,n}$	a.u.
a_1	gain fit parameter in the friendly analytical expression of L	a.u.
a_2	quenching fit parameter in the friendly analytical expression of L	a.u.
a_3	e_δ fit parameter in the friendly analytical expression of L	MeV
a_4	fractional energy loss transferred to a δ-ray, a fit parameter in the friendly analytical expression of L	
f_{geom}	light collection factor	a.u.
f_{PMT}	PMT gain factor	a.u.

2. The thallium-activated caesium iodide scintillators

2.1. The CsI(Tl) crystals of INDRA and their electronics

The 324 CsI(Tl) crystals of INDRA have thicknesses ranging between 138 and 50 mm from forward to backward angles [1]. Their temperature is stabilized at 20°C [4,5]. The CsI(Tl) crystals are coupled to photomultipliers tubes (PMT) [1] to achieve energy thresholds for mass identification lower than those obtained with photodiodes [6]. The stability control of the scintillators is ensured by means of a nitrogen laser system [1].[2] The PMT signals are fed in 24 input VXI bus modules containing the processing functions. Each channel comprises a constant fraction discriminator, two integrators for "fast" and "slow" parts with accompanying delay and gate generators. The analog-to-digital conversion is performed by two multiplexed 12-bit converters. Exhaustive descriptions of the CsI(Tl) crystals, PMTs and associated electronics, as well as of the data acquisition and triggering system are given in Refs. [1,2]. For energy calibration purpose, rings 10–17 were each equipped with a single two-element telescope (80 μm silicon and 2 mm Si(Li)

[2] Laser Science Inc., Cambridge, MA, USA.

detectors)—which will be referred to as the calibration telescope (CT). The CT covers part of one of the CsI(Tl) crystals in each backward ring.

2.2. Calculation of the deposited energy into the scintillators

For rings 2–9, the calculation of the energy deposited in a CsI(Tl) crystal, E_0, is based on the energy lost in the preceding silicon detector and on range-energy tables [8,9]. The silicon detectors were carefully calibrated taking into account the pulse-height defect, with an absolute accuracy of 2–3% [7]. However, the relative accuracy—between different ions up to Xe and for different energies up to 80 AMeV—is within 1%. For ions as light as boron, the consequent relative accuracy for the residual energy in CsI(Tl) crystal worsens from 1.3% at 50 AMeV to 3% at 5 AMeV. For xenon, the consequent relative accuracies are 1.8% at 50 AMeV and 10% at 5 AMeV. The relative accuracy of the total energy of the ion, deposited in both Si and CsI(Tl) detectors, never exceeds 2–3%. The particles are completely identified up to $Z = 4$, while for heavier fragments an hypothesis is necessary for the mass.

For rings 10–17, the CTs provide reference energy spectra. The spectrum of each reaction product is adjusted on the associated reference one. The calibration procedure for the backward rings is presented in Section 4.4, followed by a description of a rapid fragment identification recipe.

Throughout this paper, the reaction products emitted in collisions of 32 and 50 AMeV ^{129}Xe projectiles with Sn targets will be used. They cover large energy and atomic number ranges. The experimental data were taped only when at least four detectors fired. Thus, the primary reaction products originate in exit channels involving a non-negligible transfer of kinetic energy into internal degrees of freedom ($\geqslant$1.5 AMeV), leading mainly to neutron evaporation. The secondary fragments (after evaporation) populate the "attractor" line in the map of nuclides [10] rather than the "stability" line. The corresponding mass formula [10] will be employed when the isotopic mass was not determined. In most of the cases, one CsI(Tl) detector will be used (module 2 of ring 3) to illustrate the described procedure. The nominal thickness of the preceding silicon detector is 304 μm.

2.3. The shape of the signal

The light emitted by a CsI(Tl) crystal hit by a charged product has a rise time negligible [11–13] as compared to the decay time which is in the microsecond range. The rise time is related to the transfer of the energy deposited by the particle to the optical level involved into the scintillation, while the decay time constant concerns the light emission. Traditionally, the decaying part of a CsI(Tl) scintillation is described by one [14,15] or two [12] exponentials of short decay constant ($\approx$1 μs) or, more often, by one short ($\approx$1 μs) and one long (7 μs) decay-constant exponentials [16]. The short decay constant depends on the identity of the particle, while the long one is considered to be the same for all particles.

Proton-induced signals recorded by means of flash ADCs up to 20 μs [17] have shown decaying parts which are curved in a semilogarithmic scale. For very low energy (a few MeV), the shape of the decaying signal shows an exponential time dependence. At higher energy, several exponentials would be necessary for a perfect description of the shape of the whole decaying curve. The authors of Ref. [17] kept only two. The first one—the "fast component"—for the dominant steep descent part, has a short decay constant (0.5–1 μs), with a strong dependence on the atomic number Z, mass number A and incident energy E_0 of the particle. The second one—the "slow component"—has a long decay constant (5 μs) nearly independent of the type of particle. At the highest energies, the fast component covers at least $\approx$65% of the integral of the signal for hydrogen isotopes at 20–40 AMeV, $\approx$75% for helium ones at 30 AMeV, $\approx$85% for light fragments ($Z = 3$–6) at 15–25 AMeV [17] and at least 95% for heavy fragments, as shown in Fig. 1 for Si at 8 AMeV and Kr at 50 AMeV (present work). The above-mentioned weights become even more important when the incident energy E_0 decreases, i.e. when the average specific

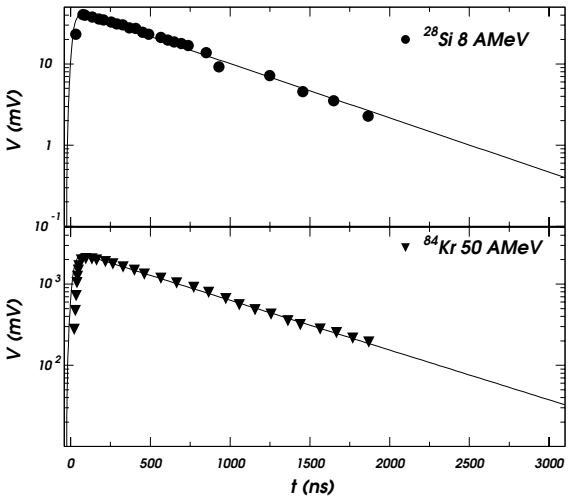

Fig. 1. The shape of the measured light signals induced by 8 AMeV ^{28}Si and 50 AMeV ^{84}Kr ions in two different CsI(Tl) crystals of INDRA—solid symbols—is well described by one exponential decaying curve provided by Eq. (3).

electronic stopping power $E_0/R(E_0)$ is high enough; $R(E_0)$ is the particle range. From the above considerations, one may assume in the latter case that only one decay constant $\tau_0(E_0, A, Z)$ is involved for each event. Its value will be close to that of the fast component.

A signal at the crystal PMT output, described as in Ref. [17] by two exponential functions associated to the fast and slow components

$$i(t) = \frac{Q_f}{\tau_f} e^{-t/\tau_f} + \frac{Q_s}{\tau_s} e^{-t/\tau_s} \quad (1)$$

has the total charge $Q_{fs} = Q_f + Q_s$ got by integrating $i(t)$ over time between 0 and ∞.

In a single exponential approximation, the same signal would be

$$i(t) = \frac{Q_0}{\tau_0} e^{-t/\tau_0} \quad (2)$$

where Q_0 approximates the integral of the signal, Q_{fs}.

3. Reconstruction of the total light output

In the case of INDRA, two parts of the signal are integrated in the time gates 0–400 ns (for the fast part F) and 1600–3100 ns (for the slow one S). Let us make the following exercise: consider the expressions of F and S provided by the two exponential formula of the signal (1) on one hand, and by the one exponential formula (2), on the other hand. The values of the expressions of F and S found in both cases have to be equal. From these equalities, one can derive τ_0 and the ratio Q_0/Q_{fs} for the data of Ref. [17], using the time gates of INDRA. The results of this estimation are plotted in Fig. 2(a) against the estimate AZ^2/E_0 of the average specific electronic stopping power, derived in the approximation—$(dE/dx)_e \propto AZ^2/E$ of the Bethe–Bloch formula. This plot has a predictive character: the maximum error done in the integral of the signal estimation would be of about 10% in the case of the most energetic protons but much lower for the charged reaction products with $Z > 1$. Fig. 2(b) shows the ratio Q_0/Q_{fs} versus the reciprocal of the decay-constant value τ_0; the normalization constant τ_{0min} is the lower measured value for ions at the lowest energies ($\approx$1 AMeV) and hence the highest stopping powers. This kind of plot could eventually be used in order to correct Q_0. In any case, as long as $AZ^2/E_0 \geqslant 0.4$ (e.g. Ar ions with $E_0/A \leqslant 810$ MeV/nucleon), Q_0 estimates Q_{fs} within 2%. This is the case for most of our data.

In view of the above argument, we shall suppose in the following that the current at the last dynode of the PMT associated to a CsI(Tl) scintillator varies exponentially in time as in Eq. (2). This current, injected in the anodic circuit of the PMT, leads to the measured current at the output of the PMT base $i_{mes}(t)$, which may be expressed [18] by means of the equation

$$i_{mes}(t) = \frac{Q_0}{\tau_0 - \tau}(e^{-t/\tau_0} - e^{-t/\tau}). \quad (3)$$

The total light output is proportional to the total charge Q_0; τ and τ_0 are the rise time and decay time constants, respectively. τ has been measured for the bases of all PMTs (60 ns for rings 11–16 and 20 ns for other rings). The shape of the signal given by Eq. (3) is shown in Fig. 1. By integrating expression (3) within the gates mentioned above,

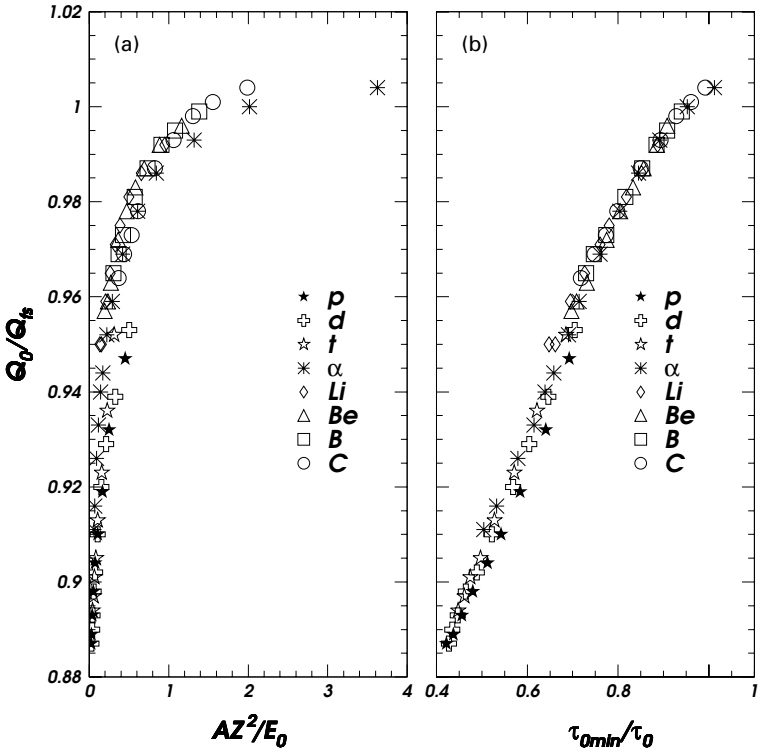

Fig. 2. Q_0 is the approximate integral of the light signal when one decaying exponential shape, of decay constant τ_0 (Eq. (2)), is assumed. Q_{fs} is the true one, corresponding to two decaying exponential shape (Eq. (1)). Their ratio increases with: (a) the estimate of the average specific electronic stopping power $\propto AZ^2/E_0$ (E_0 in MeV), (b) the inverse ratio of τ_0; τ_{0min} is a normalization constant. Processed data from Ref. [17].

one obtains

$$F = \frac{Q_0}{\tau_0 - \tau}[\tau_0(1 - e^{-t_1/\tau_0}) - \tau(1 - e^{-t_1/\tau})] \quad (4)$$

$$S \approx \frac{Q_0\tau_0}{\tau_0 - \tau}[e^{-t_2/\tau_0} - e^{-t_3/\tau_0}] \quad (5)$$

with $t_1 = 390$ ns, $t_2 = 1590$ ns and $t_3 = 3090$ ns (the integration gates have undergone a diminution of 10 ns according to the delay of the signal in the VXI cards). By means of the two Eqs. (4) and (5), the two unknown quantities τ_0 and Q_0 are calculated and therefore, within a multiplicative constant, the total experimental light output. The measured resolutions (FWHM) of the CsI(Tl) crystals for Si of 7.86 AMeV and α particles of 21 AMeV are of ≈3% for F and ≈4% for S. This leads to an accuracy of ≈1.3% for Q_0. For α particles below a total energy of 10 MeV, the accuracy progressively goes down to 3–4%, which roughly corresponds to the measured resolution on the total light at 5 MeV. For protons of 21 MeV, the resolutions (FWHM) are: ≈4% for F and ≈7% for S, leading to an accuracy of ≈2% for Q_0 above 10 MeV. Below this energy, the accuracy worsens to 6–7%.

4. Approximate formula from RNQM model

4.1. Analytical integration

In practical situations, an analytical integration of the total light output issued from the RNQM [3] would be more suited. This is possible starting

from the first-order approximation for total light output formula (expression (18) in the previous paper [3])

$$L = a_G \left[\int_0^{E_\delta} \frac{1}{1 + a_n S_n(E) + a_R S_e(E)} \times \frac{dE}{1 + S_n(E)/S_e(E)} + \int_{E_\delta}^{E_0} \frac{1 - \mathscr{F}(E)}{1 + a_n S_n(E) + a_R S_e(E)} \times \frac{dE}{1 + S_n(E)/S_e(E)} + \int_{E_\delta}^{E_0} \frac{\mathscr{F}(E)\, dE}{1 + S_n(E)/S_e(E)} \right] \quad (6)$$

if approximations are made for the stopping powers, the concentration $N_n(E)$ of the defects created by the incident fragment and the fractional energy loss $\mathscr{F}(E)$ deposited outside the primary column by the generated δ-rays. All these quantities are discussed in the preceding paper [3].

(i) For the specific electronic stopping power formula of Bethe–Bloch, the usual approximation: $(dE/dx)_e(E) = C_e AZ^2/E$, reasonable above a few AMeV, may be used; here C_e is a constant including the logarithmic term in the Bethe–Bloch formula, which varies much more slowly than $1/E$.

(ii) The created defect concentration $N_n(E)$ estimated by $N_{Ruth}(E)$, is well approximated by neglecting the second term ($\propto E^{-2}$) in Eq. (4) of the preceding paper [3] $N_n \propto AZ^2/E$.

(iii) The specific nuclear stopping power, $(dE/dx)_n(E)$, may also be roughly estimated by an AZ^2/E behaviour, as shown in Fig. 2(b) of the preceding paper [3]: $(dE/dx)_n(E) = C_n AZ^2/E$ with C_n constant. In this way, the factor $(1 + S_n(E)/S_E(E))$ in the denominator of all the terms in expression (6) becomes a constant: $1 + C_n/C_e$, to be included in the multiplicative parameter a_G that will be called a_1. The nuclear and recombination quenching terms to the denominator of the first two terms (concerning the primary column) in the same expression may be summed and replaced by only one: $a_2 AZ^2/E$.

(iv) By keeping the zero and first-order terms in the Taylor expansion around β_δ^2 of the logarithmic term of the fractional energy carried by the δ-rays (see Eq. (7) of the preceding paper [3]), one may get an approximate expression of $\mathscr{F}(\beta^2)$:

$$\mathscr{F}(\beta^2) = \frac{1}{2} \frac{(\beta^2/\beta_\delta^2) - 1}{\ln(2m_e c^2/I\ \beta_\delta^2) + \beta^2/\beta_\delta^2 - 1}. \quad (7)$$

With the above items (i)–(iv) assumptions, the first-order approximation formula (6) of the total light output depends on three parameters only and may be analytically integrated. The quality of the fragment loci reproduction in a $\Delta E_{Si} - Q_0$ map will be shown in the next subsection.

4.2. A friendly analytical formula for the total light output

The alternative to the item (iv) approximation of the fractional energy carried by the δ-rays is to consider it as a step function of energy

$$\mathscr{F}(E) = \begin{cases} 0, & E/A \leqslant a_3 \\ a_4, & E/A > a_3 \end{cases} \quad (8)$$

where a_3 is the energy per nucleon threshold for the δ-ray production and a_4 will be a fit parameter too. The advantage is that the first-order approximation of total light output expression (6) becomes very simple

$$L = a_1 \left\{ E_0 \left[1 - a_2 \frac{AZ^2}{E_0} \ln\left(1 + \frac{1}{a_2 AZ^2/E_0} \right) \right] + a_4 a_2 AZ^2 \ln\left(\frac{E_0 + a_2 AZ^2}{E_\delta + a_2 AZ^2} \right) \right\} \quad (9)$$

($E_\delta = A \times a_3$), very suitable for energy calibration purposes. The fit parameter values are given in column (a) of Table 1, and the quality of the fit is shown in Figs. 3, 4 (solid lines) and 5. Even if the total light outputs are no more as nicely reproduced as by exact calculations [3], especially for high specific electronic stopping power values, the description of the reaction product identification in the two-dimensional plot (Fig. 4) and the deviations of the calculated energies relative to the true energies (Fig. 5) remain comparable to the exact calculation case. More precisely, the heavy

Table 1
Fit parameters a_1, a_2, a_3, a_4[a]

	(a)	(b)
a_1 (a.u.)	19.5	variable
a_2 (a.u.)	0.71	0.25
a_3 (MeV/u)	3.8	3.1 (1.0)[b]
a_4	0.26	0.27

[a] The errors on the parameters (one unit on the last digit) are only statistical. The analytically integrated expression (9) of the total light output has been used: (a) values obtained by means of data concerning fragments with $Z \leqslant 45$, for a forward module ($\theta = 4.5^\circ$) of INDRA; (b) values averaged over 8 modules placed on the forward rings ($\theta \leqslant 45^\circ$), for $Z \leqslant 15$. These recommended values of a_2, a_3, a_4 to be used in Eq. (9) are suitable for all INDRA CsI(Tl) crystals.

[b] See the text for explanation.

fragment identification in a $\Delta E - Q_0$ map is possible with a resolution of one unit charge around $Z = 45$. The corresponding energy deviations may locally reach up to 15–20%, but globally they are inside $\approx 6\%$. About 3% of accuracy are lost as compared to the exact calculations. Note in Fig. 4 that the step function approximation for $\mathscr{F}$ (solid lines) does not worsen the result as compared to the physical approximation (7) (dashed lines). In fact, it is approximation (i) for the Bethe–Bloch formula which is distorting—via the fit procedure—the shape of the light response for the heaviest fragments (Fig. 3).

For the energetic light charged particles, there are discrepancies at high energy, whose origin is the slight underestimation of total light output (see Section 2.3). For energy calibration purpose, the recipe to ameliorate the situation was to use a different gain parameter a_1 for low average specific electronic stopping power ($AZ^2/E_0 < 0.4$), or directly for protons, which constitute most of the data for which the experimentally determined Q_0 differs from the real experimental light output by ≈ 2–10% (Fig. 2(a)). The alternative could be a

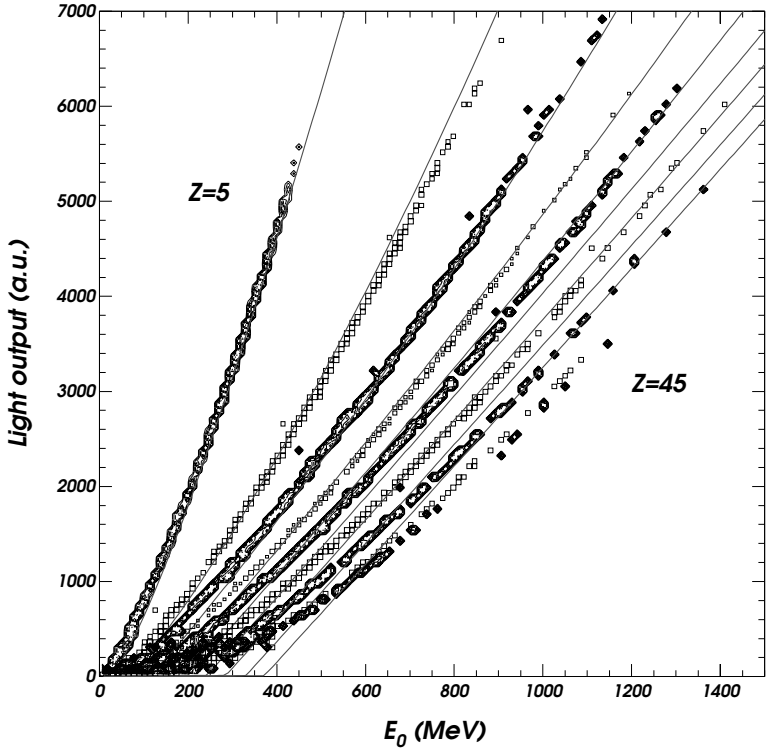

Fig. 3. Total light output against the energy for different ions ($\Delta Z = 5$): the symbols are experimental data from the system Xe + Sn at 32 and 50 AMeV; the curves are calculations done with the simple light output formula Eq. (9).

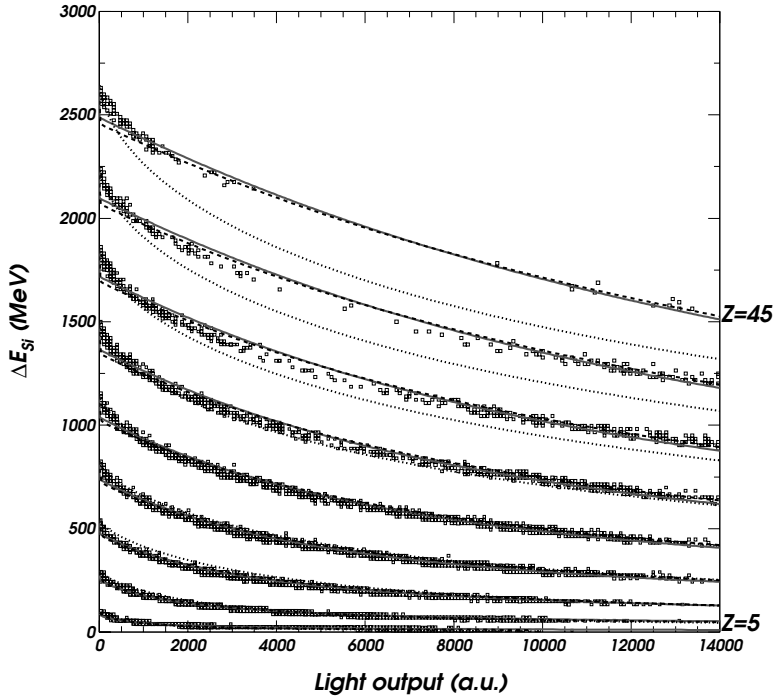

Fig. 4. A $\Delta E_{\mathrm{Si}} - Q_0$ map (module 2, ring 3 of INDRA) from the system Xe + Sn at 32 and 50 AMeV. The symbols are experimental data. For the calculated total light output, the approximations (i)–(iv) from Section 4.1 have allowed an analytical integration, by making use of two approximate expressions of $\mathscr{F}$: Eq. (7)—dashed lines—and the step function Eq. (8)—solid lines; the dotted lines are obtained if the δ-rays are completely neglected ($\mathscr{F} = 0$) (Section 4.5).

previous correction of Q_0 concerning these data, based on the $\tau_{0\min}/\tau_0$ values, as suggested by Fig. 2(b).

An interesting point is that the gain parameter values got by using only light fragments, or even light charged particles are very near the values obtained by using a large ion data range up to $Z = 45$, if the other parameters are kept constant at the values given in Table 1(a). Such a conclusion clearly appears in Fig. 6: a_1 values are found nearly independent of the upper limit in Z ($Z_{\max}$) considered. If only a_3, a_4 are kept constant at the mentioned values, a_1, a_2 remain practically the same as long as $Z_{\max} \geqslant 15$. Otherwise, as the light response induced by intermediate mass fragments or light charged particles is less non-linear than that corresponding to heavy ions, the parameter a_2 has the tendency to diminish and, consequently, a_1 too, for the same quality of the description.

A search of the fit parameter values was performed for one module of each of the 8 forward rings of INDRA ($\theta \leqslant 45^\circ$). For unitarity, we have restricted the employed data to $Z \leqslant 15$, heavy products being available only at very forward angles. Very similar values of the parameters a_3, a_4, close to those provided by large Z scale data, have been obtained. The quenching parameter a_2 is related to the average stopping power of the reaction product and also to the activator concentration of the crystal, as we shall see in the next subsection. It may vary from one ring to another, but not dramatically. The corresponding averaged values of these three parameters—presented in column (b) of Table 1—are the recommended values for the applications when formula (9) is used. a_3 was decreased at the lower detection threshold (the value in parentheses) in order to avoid the discontinuity

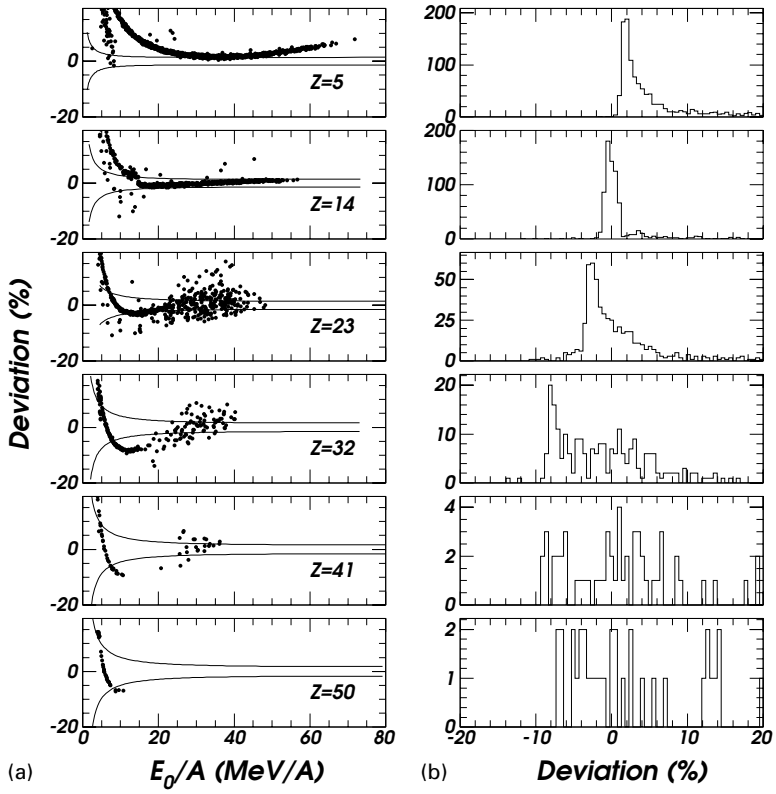

Fig. 5. Deviations (in %) of the energy values, determined with the simple light output formula Eq. (9), from the true energy values for several products of the reactions Xe+Sn at 32 and 50 AMeV: (a) deviations plotted against the product energy per nucleon: symbols; the regions between curves show the accuracy of the true energy per nucleon (see Section 2.2 for details); (b) deviation histograms.

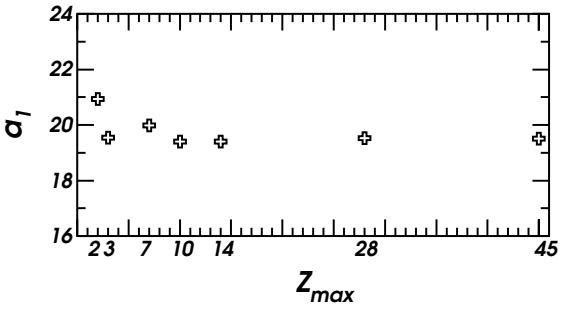

Fig. 6. Variation of the parameter a_1 as a function of the upper limit of Z considered for fit; a_2, a_3, a_4 were kept fixed with values from Table 1(a). The error bars are smaller than the symbols because only statistical errors on the parameters have been considered.

in the energy spectra induced by the "non-derivability" at $E = E_\delta$ of the light output expression as a function of the energy. By keeping a_2, a_3, a_4 fixed, the remaining gain parameter may be accurately determined as a free parameter by using simply light charged particles. The results are very similar to those shown in Figs. 3, 4 with solid lines and in Fig. 5.

4.3. Comparative study of the CsI(Tl) crystals of INDRA

Formula (9) was used to perform a comparative study of the CsI(Tl) crystals of INDRA. At forward angles (rings 2–9), the experimental values were obtained from light ions with atomic number $Z = 1$–6 and mass number A precisely identified,

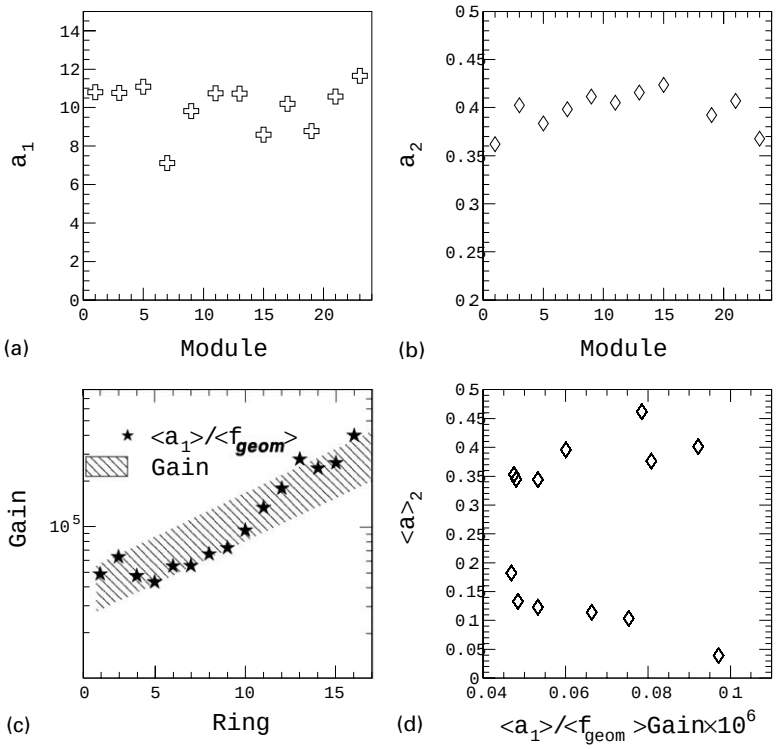

Fig. 7. (a) and (b) The fit parameters a_1, a_2 used in the simple formula (9) against the module number for ring 2 of INDRA. (c) The parameter $\langle a_1 \rangle$, averaged over all the modules of each ring and corrected for the light collection, versus the ring number; it follows the PMT gains—hatched area. (d) The quenching parameter $\langle a_2 \rangle$, averaged over the modules of each ring, versus the parameter $\langle a_1 \rangle$ corrected for light collection and PMT gain, averaged over the modules of the same ring. The error bars are smaller than the symbols because only statistical errors on the parameters have been considered.

elastically scattered by various targets. The parameters a_3, a_4, related to δ-ray production, were fixed. The crystals belonging to one ring have the same size, the same shape and similar Tl (as well as eventually defect) concentrations. The gains of the associated PMTs are the same. For this reason, one would expect that the parameters a_1 and a_2:

$$a_1 \propto f_{\text{geom}} \times f_{\text{PMT}} \times \frac{\Lambda_{\text{Ae}} N_{\text{A}}}{\Lambda_{\text{Ae}} N_{\text{A}} + \Lambda_{\text{D}} N_{\text{D}}},$$

$$a_2 \propto \frac{1}{\Lambda_{\text{Ae}} N_{\text{A}} + \Lambda_{\text{D}} N_{\text{D}}}$$

take nearly the same values for the modules of one ring; the quantities $\Lambda_{\text{Ae}} N_{\text{A}}, \Lambda_{\text{D}} N_{\text{D}}$ were defined in the previous paper [3] and f_{geom}, f_{PMT} are factors connected to the light collection (geometry of the crystal) and to the PMT gain, respectively. Actually, this is the situation, as shown in Fig. 7(a) and (b) for the modules of ring 2.

If $\Lambda_{\text{D}} N_{\text{D}} / \Lambda_{\text{Ae}} N_{\text{A}} \ll 1$, the parameter a_1 / f_{geom} is mainly related to the associated PMT gain. The geometrical light collection factor f_{geom} is proportional to the response of the crystal at ^{137}Cs source γ-ray irradiation measured with the same PMT for all the crystals of INDRA [1]. Averaged over the modules of the same ring, the parameter $\langle a_1 \rangle / \langle f_{\text{geom}} \rangle$ plotted versus the ring number, follows the approximately known values of the PMT gains (provided by the manufacturer) as shown in Fig. 7(c). The correlation of the two parameters $\langle a_1 \rangle$ and $\langle a_2 \rangle$ may be followed in Fig. 7(d), if $\langle a_1 \rangle$ is previously corrected for the geometric and gain factors. Obviously, there is no mathematical correlation: two groups of detectors are put in evidence. They may correspond to

different concentrations of the Tl activator—from 200 to 2000 ppm—(and eventually of the other crystal imperfections) which could appear during the CsI(Tl) crystal growth through the Bridgman method.[3]

The above statistics performed over more than 300 CsI(Tl) crystals belonging to the INDRA array enforce the consistency of the RNQM and of the exact or approximate light output expressions obtained in its framework. The parameters a_3, a_4 and, to a certain extent, a_2 may be considered as intrinsic characteristics of the CsI(Tl) scintillators used in nuclear physics applications. Insofar, the rather simple formula (9) of the total light output, together with the recommended values in Table 1(b) constitute a powerful tool to be used in heavy ion experiments. It should be however noted that these values are only valid as long as the time dependence of the CsI(Tl) signals is not altered by the PMT [1]. Starting from easily obtained light charged particle experimental data (excluding protons if their total light signal is not directly measured), they allow to accomplish useful applications such as heavy fragment identification and their energy determination. An example is given in the following subsection.

4.4. Reaction product identification and energy calibration of the backward angle modules of INDRA

There are two major difficulties when the CsI(Tl) scintillators of INDRA placed at polar angles above 45° are exploited. Firstly, in a $\Delta E_{IC} - Q_0$ map the identification is perfect for low atomic number, Z, of the fragments ($Z \leqslant 15$), but it becomes uncertain for higher Z values because of the poor statistics and the low IC energy resolution. Secondly, at large angles it is quite difficult to obtain elastic scattering data for fragments. Insofar, the calibration of the module belonging to the same ring is performed in two stages.

In the first stage, we consider the CsI(Tl) partially obturated by the calibration telescope CT. Most of the fragments ($Z \geqslant 4$) are stopped in the Si(Li) and therefore identified in the Si–Si(Li) telescope. The corresponding energy spectra are built for each atomic number Z. Energetic light charged particles (> 20 AMeV) pass through the silicon telescope and stop in the CsI(Tl) crystal coupled behind. With the analytical expression (9) of the light output, and the values from Table 1(b) for parameters a_2, a_3 and a_4, the parameter a_1 is determined by a fit procedure. By means of these parameters, the energy spectrum in the scintillator is built for each of the light charged particles punching through the silicon telescope. Put together the silicon telescope and CsI(Tl) scintillator spectra provide the whole energy spectrum for a given particle. These spectra and those of fragments up to $Z = 15$ stopped in the Si–Si(Li) telescope are the reference spectra for the respective ring. At the same time, the parameters allow to perform Z identification in a $\Delta E_{IC} - Q_0$ map for the whole range of atomic number of light charged particles and fragments passing beside the silicon telescope and entering the CsI(Tl) coupled behind. The energy spectra of these reaction products were compared with the reference spectra; the superposition is quite good.

In the second stage all the other CsI(Tl) scintillators of the ring are calibrated. The energy spectra for a given Z have to be identical to the corresponding reference one (the trigger used in the experiments did not break the axial symmetry of INDRA). Each light response spectrum is thus adjusted on the reference spectrum. A χ^2 minimizing procedure based on the MINUIT package from CERN library is used. It provides the parameters a_1, for the considered module. The parameters a_i ($i = 1, 4$) allow afterwards to extrapolate the Z identification in the $\Delta E_{IC} - Q_0$ map [19]. The good quality of the procedure is illustrated in Fig. 8, where energy spectra of different particles stopped in one of the scintillators of ring 10 of INDRA are compared to the reference spectra of the same ring.

4.5. And if the δ-rays would be neglected?

We have to stress once again the importance of taking into account the δ-ray effect in the light

[3] BDH-Merck Ltd, West Quay Rd, Poole, BH15 1HX, England.

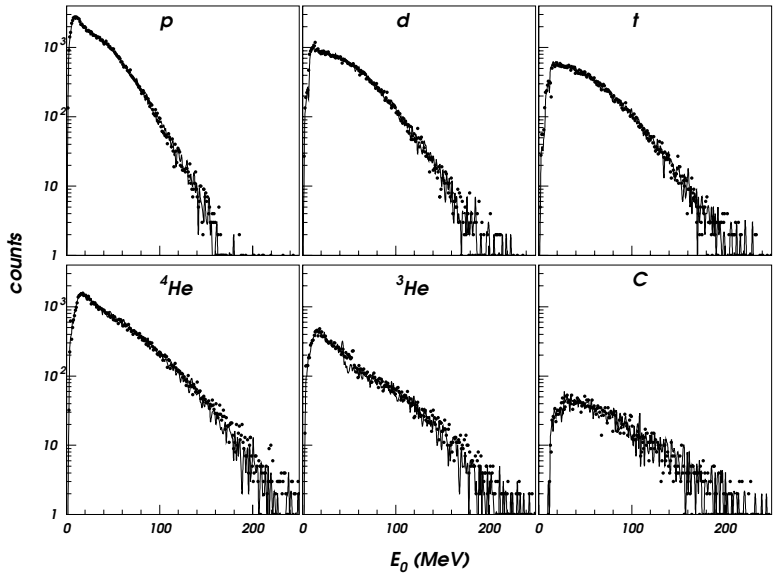

Fig. 8. Energy spectra of light charged particles and fragments in one of the CsI(Tl) crystal of ring 10 of INDRA (symbols). They are compared to the same charged reaction product energy spectra of the reference module (lines) of this ring.

output, especially for heavy reaction products ($Z \geqslant 15$). By neglecting it, only the first term on the right-hand side of Eq. (9) would appear. The results remain reasonable for $Z \leqslant 15$ but with significantly different values of the fit parameters. The quality of the fit is drastically degraded for fragments heavier than $Z = 15$. So are particle identification (Fig. 4) and energy calibration.

5. Conclusions

The data obtained with the INDRA array (large range in Z and E_0) provided a good opportunity to proceed to a basic study of the light output of CsI(Tl) scintillators and to derive suitable calibration and identification procedures. Starting from the fast and slow parts of the light output, it was possible to rebuild the integral of the signal.

Under suitable approximations, the expression of the total light output derived in the preceding paper [3] may be analytically integrated. Even if up to 3% of the accuracy may be lost, the fact presents the huge advantage of extremely short computing time. The derived expression, easy to handle, was successfully applied for fragment identification in $\Delta E_{\mathrm{Si,IC}} - Q_0$ maps and for the energy calibration of the CsI(Tl) scintillators. At forward angles, where a Si detection layer exists, these applications lead to an important reduction of the computing time. At backward angles, where two problems exist: fragment identification and energy calibration of the CsI(Tl) crystals, the above procedure plays an even more important role and corresponds to the optimum way we have found to solve these two tasks.

A comparative study of the CsI(Tl) scintillators of INDRA has shown that the model parameters are meaningful quantities, related to the light collection and the PMT gain, to the activator and eventually crystal imperfection concentrations and to the δ-ray production. All but the gain parameter are characteristics of the usual CsI(Tl) scintillators. Their averages, performed over the 324 CsI(Tl) crystals of INDRA, allowed to find reliable, recommended parameter values. Together with the related total light expression, they constitute good implements for energy calibration and heavy ion identification applications in heavy ion physics experiments.

References

[1] J. Pouthas, et al., Nucl. Instr. and Meth. A 357 (1995) 418.
[2] J. Pouthas, et al., Nucl. Instr. and Meth. A 369 (1996) 222.
[3] M. Parlog et al., Nucl. Instr. and Meth. A 482 (2002), this issue.
[4] D. Williams, G.F. Snelling, J. Pickup, Nucl. Instr. and Meth. 39 (1966) 141.
[5] D.W. Stracener, et al., Nucl. Instr. and Meth. A 294 (1990) 485.
[6] D. Guinet, et al., Nucl. Instr. and Meth. A 278 (1989) 614.
[7] G. Tabacaru, et al., Nucl. Instr. and Meth. A 428 (1999) 379.
[8] F. Hubert, R. Bimbot, H. Gauvin, At. Data Nucl. Data Tables 46 (1990) 1.
[9] L.C. Northcliffe, R.F. Schillling, Nucl. Data Tables A7 (1970) 233.
[10] R.J. Charity, Phys. Rev. C 58 (1998) 1073.
[11] V.K. Liapidevski, et al., PTE 2 (1974) 62.
[12] H. Grassmann, E. Lorentz, H.G. Moser, Nucl. Instr. and Meth. A 228 (1985) 323.
[13] J.D. Valentine, W.M. Moses, S.E. Derenzo, D.K. Wehe, G.F. Knoll, Nucl. Instr. and Meth. A 325 (1993) 147.
[14] J.C. Robertson, J.G. Lynch, W. Jack, Proc. Phys. Soc. 78 (1961) 1188.
[15] J.C. Robertson, J.G. Lynch, Proc. Phys. Soc. 77 (1961) 751.
[16] R.S. Storey, W. Jack, A. Ward, Proc. Phys. Soc. 72 (1958) 1.
[17] F. Benrachi, et al., Nucl. Instr. and Meth. A 281 (1989) 137.
[18] G.F. Knoll, Radiation Detection and Measurements, 3rd Edition, Wiley, New York, 2000, p. 229.
[19] N. Le Neindre, Thèse docteur de l'Université de Caen, 1999, LPCC T 99-02.